

# DATA-DRIVEN SPECTRAL ANALYSIS THROUGH PSEUDO-RESOLVENT KOOPMAN OPERATOR IN DYNAMICAL SYSTEMS

Yuanchao Xu<sup>1\*</sup>† Itsushi Sakata<sup>2\*</sup> Isao Ishikawa<sup>1</sup>

<sup>1</sup> Center for Science Adventure and Collaborative Research Advancement (SACRA)  
Graduate School of Science, Kyoto University

<sup>2</sup> RIKEN Center for Advanced Intelligence Project

## ABSTRACT

We present a data-driven method for spectral analysis of the Koopman operator based on direct construction of the pseudo-resolvent from time-series data. Finite-dimensional approximation of the Koopman operator, such as those obtained from Extended Dynamic Mode Decomposition, are known to suffer from spectral pollution. To address this issue, we construct the pseudo-resolvent operator using the Sherman-Morrison-Woodbury identity whose norm serves as a spectral indicator, and pseudoeigenfunctions are extracted as directions of maximal amplification. We establish convergence of the approximate spectrum to the true spectrum in the Hausdorff metric for isolated eigenvalues, with preservation of algebraic multiplicities, and derive error bounds for eigenvalue approximation. Numerical experiments on pendulum, Lorenz, and coupled oscillator systems demonstrate that the method effectively suppresses spectral pollution and resolves closely spaced spectral components.

## 1 Introduction

The study of nonlinear dynamical systems is central to many scientific and engineering problems [1, 2, 12, 22, 24, 25]. Traditionally, their analysis relies on first-principles models together with tools such as phase-space geometry [22], perturbation methods [11] for weak nonlinearities, and direct numerical simulation. These approaches have delivered deep insight, but they can be difficult to use when an accurate governing model is unavailable, when model parameters are uncertain, or when the goal is to infer global dynamical features from observations rather than describe local behavior near equilibria [7, 8]. Meanwhile, modern experiments and simulations increasingly produce large amount of time-series measurements, which has attracted growing interest in data-driven methods that aim to characterize dynamical behavior directly from data.

A natural perspective for data-driven analysis is to focus on the evolution of observable quantities rather than the underlying state variables. In many applications, one does not have direct access to the full state of a system but instead observations of the state, e.g., temperatures, velocities, concentrations, or other quantities of interest. The Koopman operator provides a mathematical framework for this viewpoint; more specifically, it describes how observables evolve in time by composing them with the flow map of the dynamical system [15, 16, 19]. Although the underlying dynamics may be nonlinear, the Koopman operator acts linearly on the space of observables, enabling spectral analysis to reveal dynamical features such as oscillation frequencies, growth and decay rates, and coherent structures. Dynamic Mode Decomposition (DMD) [27] and its extension, Extended Dynamic Mode Decomposition (EDMD) [28], provide practical algorithms for approximating the Koopman operator and its spectral properties directly from time-series data, and theoretical foundations have established convergence of these approximations under appropriate conditions [4, 10, 14, 17, 30].

Despite these convergence guarantees, a fundamental difficulty arises when extracting spectral information from finite-dimensional approximations: the phenomenon of spectral pollution [4]. The approximating matrix is finite-dimensional and therefore possesses a discrete spectrum, whereas the true Koopman operator may have continuous

\*Corresponding Authors. Email to: xu.yuanchao.3a@kyoto-u.ac.jp

†Equal Contributions.

spectral components including continuous spectrum [18]. Consequently, computed eigenvalues may include spurious points that do not correspond to any part of the true spectrum, in other words, these are drawbacks of the finite-dimensional truncation rather than intrinsic dynamical features. Conversely, true spectral points may be missed entirely if they are not well-represented by the chosen dictionary. This problem is not merely a matter of insufficient data or dictionary size; it is a structural consequence of approximating an infinite-dimensional operator by finite-dimensional matrices.

To address spectral pollution, Residual Dynamic Mode Decomposition [4] was introduced to validate candidate eigenvalues by computing residuals of approximate eigenfunctions. The key insight is that small residuals provide a certificate that a computed eigenvalue lies near the true spectrum, while large residuals indicate potential spectral pollution. This approach achieves rigorous convergence to spectral measures of the Koopman operator and provides a mathematically prominent framework for spectral computation. However, its implementation requires careful estimation of approximation errors associated with finite-dimensional projections, as these errors can be sensitive to the choice of dictionary and to the underlying spectral structure.

In this paper, we explore an alternative approach based on direct construction of the pseudo-resolvent operator from data [6, 9, 11, 26]. The resolvent encodes complete spectral information through its operator norm, which becomes large precisely when the spectral parameter approaches the spectrum. We show that the Sherman-Morrison-Woodbury identity enables efficient computation of the pseudo-resolvent directly from data matrices, and we extract pseudoeigenfunctions as directions of maximal amplification under this operator. We establish convergence of the approximate spectrum to the true spectrum in the Hausdorff metric with preservation of algebraic multiplicities, and derive computable error bounds for eigenvalue approximations [3, 11, 20]. Numerical experiments on pendulum, Lorenz, and coupled oscillator systems demonstrate the effectiveness of the method in suppressing spectral pollution and resolving closely spaced spectral components.

The remainder of this paper is organized as follows. Section 2 reviews the necessary background on Koopman operators, resolvents, and pseudo-resolvents. Section 3 presents the data-driven construction of the pseudo-resolvent matrix. Section 4 develops the convergence theory, including Hausdorff convergence of spectra and conditions for multiplicity preservation. Section 5 derives error bounds controlled by computable residual quantities. Section 6 presents numerical experiments on pendulum, Lorenz, and coupled oscillator systems. Section 7 concludes with a discussion of the method’s scope and directions for future work.

## 2 Preliminary

### 2.1 Koopman Operator

The Koopman operator is a cornerstone of modern dynamical systems theory, offering a linear framework to study the evolution of nonlinear systems. Consider a dynamical system defined on the state space  $\mathcal{M}$  equipped with a measure  $\mu$  (which is not necessarily invariant), and let  $T : \mathcal{M} \rightarrow \mathcal{M}$  be the transformation map. The bounded Koopman operator  $\mathcal{K}$  associated with  $T$  acts on the space of square-integrable functions  $\mathcal{F} := L^2(\mathcal{M}, \mu)$ , with the inner product defined by  $\langle f, g \rangle := \int_{\mathcal{M}} \bar{f}g \, d\mu$ , is given by

$$\mathcal{K}f(x) = f(T(x)), \quad \forall f \in \mathcal{F}, \quad \forall x \in \mathcal{M}.$$

In our framework, the analysis and convergence results are primarily developed for this discrete-time Koopman operator  $\mathcal{K}$ .

It is important to note that many dynamical systems are naturally continuous in time. In such cases, the dynamics are described by a flow  $\{T_t\}_{t \geq 0}$  and the corresponding Koopman operator generalizes to a one-parameter semigroup  $\{\mathcal{K}^t\}_{t \geq 0}$  defined by

$$\mathcal{K}^t f(x) = f(T_t(x)), \quad \forall f \in \mathcal{F}, \quad t \geq 0.$$

Under standard assumptions, e.g.,  $C_0$  semigroup [5, 21], this Koopman semigroup has a closed and densely defined generator  $\mathcal{A}$  such that  $\mathcal{K}^t = e^{t\mathcal{A}}$  for  $t \geq 0$ . In our study, the discrete-time operator  $\mathcal{K}$  is viewed as the embedded system obtained by sampling the continuous-time flow at unit time  $t = 1$ , i.e.,

$$\mathcal{K} = \mathcal{K}^1. \tag{1}$$

This relationship allows us to leverage the rich theoretical framework of discrete approximation for convergence analysis while establishing a direct connection to the continuous-time dynamics. In the pendulum example of Section 6.1, the first and second Figures 1, 2 are based on the discrete operator  $\mathcal{K}$  (or its finite-dimensional approximation), whereas the third Figure 3 investigates the continuous-time generator. This dual perspective ensures that our discrete framework not

only rigorously captures the spectral properties of  $\mathcal{K}$  but also provides a pathway to understand the continuous-time dynamics via this embedding as in Eq. (1).

The power of the Koopman operator lies in its ability to linearize nonlinear dynamics: even when  $T$  is highly nonlinear,  $\mathcal{K}$  induces a linear evolution on  $\mathcal{F}$ . Spectral analysis of  $\mathcal{K}$  through its eigenvalues, eigenfunctions, and invariant subspaces reveals critical dynamical properties such as periodicity, mixing, and chaos. For a contractive  $\mathcal{K}$ , its spectrum  $\sigma(\mathcal{K})$  lies within the closed unit disk. When considering the continuous-time generator  $\mathcal{A}$ , the spectrum is typically confined to the left half-plane,  $\text{Re}(z) \leq 0$ , which reflects dissipative dynamics.

Moreover, under appropriate conditions, the spectral mapping theorem provides a rigorous link between the spectrum of the generator  $\mathcal{A}$  and that of the semigroup  $\{\mathcal{K}^t\}_{t \geq 0}$ . In particular, when  $\mathcal{K}^t = e^{t\mathcal{A}}$  and  $t = 1$ , the theorem asserts that

$$\sigma(\mathcal{K}) = \{e^\lambda : \lambda \in \sigma(\mathcal{A})\},$$

provided that  $\mathcal{K}$  is bounded and  $\mathcal{A}$  generates a strongly continuous semigroup. This relationship not only validates the discrete-time framework (where  $\mathcal{K} = \mathcal{K}^1$ ) as an embedded representation of the continuous-time dynamics but also enables the computation of the generator's spectral properties via the more accessible spectrum of  $\mathcal{K}$ .

In practice, the Koopman operator is particularly valuable in data-driven analysis, as it allows one to approximate  $\mathcal{K}$  directly from time-series data without requiring an explicit model for  $T$ . This approach has been successfully applied in diverse fields such as fluid dynamics, neuroscience, and statistical mechanics, where the evolution of observables is often more accessible than tracking individual trajectories.

## 2.2 Resolvent and Pseudo-Resolvent Operator

The resolvent is a fundamental concept in operator theory, particularly for linear operators on the space  $\mathcal{F}$ . For a linear operator  $\mathcal{A}$  (possibly unbounded) defined on a dense subspace of  $\mathcal{F}$ , its spectrum  $\sigma(\mathcal{A})$  consists of all complex numbers  $z$  for which  $zI - \mathcal{A}$  (with  $I$  the identity operator) is not invertible. The resolvent set  $\rho(\mathcal{A})$  is the complement of  $\sigma(\mathcal{A})$  in  $\mathbb{C}$ , i.e. those  $z$  where  $zI - \mathcal{A}$  has a bounded inverse. The resolvent of  $\mathcal{A}$  at  $z \in \rho(\mathcal{A})$  is the operator  $\mathcal{R}(z, \mathcal{A}) = (zI - \mathcal{A})^{-1}$ , which maps  $\mathcal{F}$  into the domain  $\mathcal{D}(\mathcal{A})$  of  $\mathcal{A}$ . This operator  $\mathcal{R}(z, \mathcal{A})$  is bounded and provides a way to "resolve" the equation  $(zI - \mathcal{A})f = g$  by giving  $f = \mathcal{R}(z, \mathcal{A})g$  whenever  $z$  lies outside the spectrum. The resolvent  $\mathcal{R}(z, \mathcal{A})$  has several useful properties. It is an analytic (holomorphic) function of  $z$  on  $\rho(\mathcal{A})$ , often expressible via a Neumann series when  $|z|$  is large or  $z$  is near some  $z_0 \in \rho(\mathcal{A})$ . It also satisfies the *first resolvent identity*: for any  $z, \mu \in \rho(\mathcal{A})$ ,

$$\mathcal{R}(z, \mathcal{A}) - \mathcal{R}(\mu, \mathcal{A}) = (\mu - z) \mathcal{R}(z, \mathcal{A}) \mathcal{R}(\mu, \mathcal{A}),$$

which can be verified by manipulating  $(zI - \mathcal{A})^{-1} - (\mu I - \mathcal{A})^{-1}$  and factoring out  $(\mu - z)$ . This identity is central to understanding the continuity and differentiability of  $\mathcal{R}(z, \mathcal{A})$  and links  $\mathcal{R}(z, \mathcal{A})$  to the spectral properties of  $\mathcal{A}$ . For instance, if  $\mathcal{A} = \mathcal{K}$  is the Koopman operator on  $\mathcal{F}$  and  $\mathcal{K}$  is contractive, then the spectrum  $\sigma(\mathcal{K})$  lies inside the unit disk, and the resolvent  $\mathcal{R}(z, \mathcal{K})$  exists (is bounded) for all  $|z| > 1$ . This provides a window into the frequencies or growth/decay rates of the dynamical system underlying  $\mathcal{K}$ .

A generalization of the resolvent operator is the pseudo-resolvent, which extends the framework beyond cases where a well-defined generating operator exists. A family of operators  $\{\mathcal{R}(z)\}_{z \in \Omega}$ , where  $\Omega$  is a subset of the complex plane  $\mathbb{C}$ , is called a pseudo-resolvent if it satisfies the *first resolvent identity*:

$$\mathcal{R}(z) - \mathcal{R}(\mu) = (\mu - z) \mathcal{R}(z) \mathcal{R}(\mu), \quad \forall z, \mu \in \Omega.$$

This definition does not assume the existence of an operator  $\mathcal{A}$  such that  $\mathcal{R}(z) = (zI - \mathcal{A})^{-1}$ . When such an operator exists, the pseudo-resolvent is said to be representable.

Pseudo-resolvents maintain many important properties of standard resolvents, including analyticity on their domain of definition. The domain of a pseudo-resolvent, analogous to the resolvent set, consists of points  $z \in \mathbb{C}$  where  $\mathcal{R}(z)$  exists as a bounded operator. The spectrum associated with a pseudo-resolvent can still be defined as the complement of this domain in  $\mathbb{C}$ .

The flexibility of pseudo-resolvents makes them particularly valuable in data-driven contexts, where the underlying operator might not be explicitly available or might not exist in the classical sense. In such settings, constructing a family of operators that satisfies the resolvent identity often provides sufficient analytical power, even without an explicit representation in terms of a generating operator. This approach is especially relevant for complex dynamical systems where complete knowledge of the system's operator or generator may be unavailable, but data-driven approximations can still capture essential spectral characteristics of the dynamics.

### 3 A Data-Driven Computational Approach for Pseudo-Resolvent Estimation

Recall that the EDMD-approximated Koopman operator(semigroup) matrix  $\mathbf{K}_N$  [28] and generator matrix  $\mathbf{A}_N$  [14] are:

$$\mathbf{K}_N = \Psi_X^\dagger \Psi_Y \quad \mathbf{A}_N = \Psi_X^\dagger \Psi'_X, \quad (2)$$

where  $\Psi_X, \Psi_Y \in \mathbb{C}^{M \times N}$  are  $N$  basis evaluations at  $M$  data points,  $\Psi'_X = (\Psi_Y - \Psi_X)/\Delta t$  and  $\Psi_X^\dagger$  is pseudoinverse of  $\Psi_X$ .

**Remark 3.1.** Alternatively, one can also apply Itô formula to compute each elements in the matrix  $\Psi'_X$  if the system is stochastic. See [14, 30] for more details.

The **Sherman-Morrison-Woodbury (SMW)** [29] identity is the following:

$$(A + UV)^{-1} = A^{-1} - A^{-1}U(I + VA^{-1}U)^{-1}VA^{-1} \quad (3)$$

For each  $z \in \mathbb{C}$ , apply Eq. (3) to the pseudo-resolvent matrix  $(zI - \Psi_X^\dagger \Psi_Y)^{-1}$  with  $A = zI, U = -\Psi_X^\dagger, V = \Psi_Y$ , we have

$$\mathbf{R}_N(z) := \frac{1}{z}I + \frac{1}{z^2}\Psi_X^\dagger(I - \frac{1}{z}\Psi_Y\Psi_X^\dagger)^{-1}\Psi_Y. \quad (4)$$

Note that, the construction of pseudo-resolvent matrix  $\mathbf{R}_N(z)$  is equivalent to the resolvent matrix  $\mathbf{R}(z, \mathbf{K}_N)$  by Eq.(2); specifically,

$$\mathbf{R}_N(z) = (zI - \Psi_X^\dagger \Psi_Y)^{-1} = (zI - \mathbf{K}_N)^{-1} = \mathbf{R}(z, \mathbf{K}_N) \quad (5)$$

Thus, by Eq.(5), we can verify matrix identity for difference of inverses in the following:

$$\begin{aligned} \mathbf{R}_N(z) - \mathbf{R}_N(w) &= (zI - \mathbf{K}_N)^{-1} - (wI - \mathbf{K}_N)^{-1} \\ &= (zI - \mathbf{K}_N)^{-1}[(wI - \mathbf{K}_N) - (zI - \mathbf{K}_N)](wI - \mathbf{K}_N)^{-1} \\ &= (w - z)\mathbf{R}_N(z)\mathbf{R}_N(w) \end{aligned}$$

Analogously, the corresponding pseudo-resolvent matrix  $(zI - \Psi_X^\dagger \Psi'_X)^{-1}$  for a generator study in a continuous time setting is given by:

$$\begin{aligned} \mathbf{R}_N(z) &:= \frac{1}{z}I + \frac{1}{z^2}\Psi_X^\dagger(I - \frac{1}{z}\Psi'_X\Psi_X^\dagger)^{-1}\Psi'_X \\ &= (zI - \Psi_X^\dagger \Psi'_X)^{-1} = (zI - \mathbf{A}_N)^{-1} = \mathbf{R}(z, \mathbf{A}_N). \end{aligned} \quad (6)$$

**Remark 3.2.** In this paper, we will use notation  $\mathbf{R}_N(z)$  for both  $\mathbf{R}(z, \mathbf{K}_N)$  and  $\mathbf{R}(z, \mathbf{A}_N)$ , depending on the context of discussion.

The matrix approximation  $\mathbf{R}_N(z)$  can be viewed as a pseudo-resolvent operator approximation since this construction is entirely data-driven, working directly with the data matrices rather than requiring an explicit construction of the matrix representation  $\mathbf{K}_N$  of Koopman operator approximation  $\mathcal{K}_N$  first. Simultaneously, due to the mathematical equivalence established through the Sherman-Morrison-Woodbury formula, this matrix approximation  $\mathbf{R}_N(z)$  is mathematically equivalent to a standard resolvent operator approximation  $\mathbf{R}(z, \mathbf{K}_N) = (zI - \mathbf{K}_N)^{-1}$ . This equivalence ensures that all the theoretical results proven in Section 4 of the paper—including norm resolvent convergence property, spectral boundary stability, and Hausdorff distance convergence—remain valid and applicable. In this interpretation, we can leverage the theoretical foundations developed for standard resolvent operators while maintaining the practical benefits of a directly data-driven construction that aligns with pseudo-resolvent formulations.

### 4 Convergence Analysis of Spectrum

**Definition 4.1.** Denote  $\sigma(\mathcal{K})$  the spectrum of bounded Koopman operator  $\mathcal{K}$ . Let  $\mathcal{K}_N$  be a sequence of finite-dimensional discretized operators approximating  $\mathcal{K}$  due to the discretization by Galerkin approximation [17, 28]. The resolvent operator  $\mathcal{R}(z)$  is defined as:

$$\mathcal{R}(z) := \mathcal{R}(z, \mathcal{K}) = (zI - \mathcal{K})^{-1},$$

for  $z \in \rho(\mathcal{K})$ , where  $\rho(\mathcal{K})$  is the resolvent set of  $\mathcal{K}$  [11].

For the finite-dimensional approximation  $\mathcal{K}_N$ , we define a data-driven approximation of the pseudo-resolvent operator  $\mathcal{R}_N(z)$  whose matrix representation in the chosen dictionary is given by the large data limit  $\lim_{M \rightarrow \infty} \mathbf{R}_N(z)$  as formulated in Eq.(4). This approximation is valid for all  $z \in \rho(\mathcal{K}_N)$ , where  $\rho(\mathcal{K}_N)$  is the resolvent set of  $\mathcal{K}_N$ .

Notice that the convergence of  $\lim_{M \rightarrow \infty} \mathbf{R}_N(z)$  in large data is guaranteed by examining its structure in Eq.(4). This expression can be expanded as a Neumann series where each term involves powers of the Koopman operator matrix. According to EDMD theory [17, 28], these matrices converge almost surely in the large data limit  $M \rightarrow \infty$ , where  $M$  represents the number of data points. Specifically, under appropriate sampling conditions, the empirical averages(i.e., the two Gram matrices formed by Galerkin approximation) in the EDMD procedure converge to their expected values by the Strong Law of Large Numbers(SLLN), ensuring that our pseudo-resolvent operator approximation  $\mathcal{R}_N(z)$  is well-defined and reliable for spectral analysis. Moreover, since  $\mathcal{K}$  is bounded,  $\mathcal{K}_N \rightarrow \mathcal{K}$  in strong operator topology as proved in [17, Theorem 3] However, this does not implies the same convergence type for  $\mathcal{R}_N(z) \rightarrow \mathcal{R}(z)$ . It is only true with extra condition, as we will discuss about later.

Let  $\mathcal{R}_N(z)$  be the (finite dimensional) pseudo-resolvent operator whose matrix representation is given in Eq.(4). Due to Eq.(5), we know that

$$\mathcal{R}_N(z) = \mathcal{R}(z, \mathcal{K}_N) = (zI - \mathcal{K}_N)^{-1}.$$

**Assumption 4.2.** For any  $z \in \rho(\mathcal{K})$  there exists  $N(z)$  such that for all  $N > N(z)$ , we have

$$\|\mathcal{R}_N(z)\| \leq M_z, \quad (7)$$

for some  $M_z < \infty$ .

Assumption 4.2 is usually called *stable convergence* [3, Chapter 3.4]. It acts as a stability condition that prevents ill-conditioning in the approximation process. Without such a condition, spectral approximation could produce spurious eigenvalues or fail to capture the true spectral properties of the original operator.

**Remark 4.3.** Recall *second resolvent identity*:  $\mathcal{R}_N(z) - \mathcal{R}(z) = \mathcal{R}_N(z)(\mathcal{K} - \mathcal{K}_N)\mathcal{R}(z)$ . By Eq.(7) and the *second resolvent identity*, we obtain a strong convergence for  $\mathcal{R}_N(z)$ , i.e., for each  $z \in U \subset \rho(\mathcal{K})$ , there exists  $N_z \in \mathbb{N}$  such that for  $N > N_z$ ,

$$\mathcal{R}_N(z)f \rightarrow \mathcal{R}(z)f, \quad \forall f \in \mathcal{F} \quad (8)$$

**Definition 4.4.** Let  $\lambda$  be an isolated eigenvalue of  $\mathcal{K}$  with algebraic multiplicity  $m_\lambda < \infty$  and  $\Gamma_\lambda$  be a closed Jordan curve around  $\lambda$  containing no other point of  $\sigma(\mathcal{K})$ . Define the spectral projection  $\mathcal{P}^\lambda, \mathcal{P}_N^\lambda$  associated with  $\lambda$  as:

$$\mathcal{P}^\lambda := \frac{1}{2\pi i} \int_{\Gamma_\lambda} \mathcal{R}(z) dz, \quad \mathcal{P}_N^\lambda := \frac{1}{2\pi i} \int_{\Gamma_\lambda} \mathcal{R}_N(z) dz.$$

Let  $\dim \mathcal{P}^\lambda \mathcal{F}, \dim \mathcal{P}_N^\lambda \mathcal{F}$  be the invariant subspace under the projection  $\mathcal{P}, \mathcal{P}_N$ .

**Assumption 4.5.** Let  $\lambda \in \sigma(\mathcal{K})$  be an isolated eigenvalue with algebraic multiplicity  $m_\lambda$ . Assume  $\dim \mathcal{P}_N^\lambda \mathcal{F} = \dim \mathcal{P}^\lambda \mathcal{F} = m_\lambda < \infty$  for all large  $N$ .

Assumption 4.5 is usually called *strongly stable convergence* [3, Chapter 5] which is essential for multiplicity preservation in the spectral convergence. This assumption is valid since we will later show that  $\dim \mathcal{P}_N^\lambda \mathcal{F} \geq m_\lambda$  whenever  $N$  is large enough in Corollary 4.9.

In the next Lemma 4.6, we will show a uniform bound for  $\mathcal{R}_N(z)$  over a compact subset of  $\rho(\mathcal{K})$ .

**Lemma 4.6.** Let  $U$  be a compact subset of the resolvent set  $\rho(\mathcal{K})$ . If Eq.(7) from Assumption 4.2 holds for all  $z \in U$ , then there exists  $N_U \in \mathbb{N}$  and a constant  $M_U < \infty$  such that

$$\sup_{z \in U, N > N_U} \|\mathcal{R}_N(z)\| \leq M_U.$$

*Proof.* First, we show that  $\mathcal{R}(z)$  is continuous in  $z \in U$  and uniformly in  $N$  for  $N$  large enough.

Denote  $M_z = \sup_{N > N_z} \|\mathcal{R}_N(z)\| < \infty$ , which is finite for each  $z$ . For any  $\varepsilon > 0$ , since  $U$  is a compact subset of  $\rho(\mathcal{K})$ ,  $U$  can be covered by a finite number  $J$  of open balls  $\{B(z_j, \varepsilon)\}_{j=1}^J$ , where  $z_j \in U$ . Then, for each  $z_j$ , Eq.(7) ensures there exists  $N_{z_j}$  such that for  $N > N_{z_j}$ ,  $\|\mathcal{R}_N(z_j)\| \leq M_{z_j} < \infty$ . Define  $N_0 = \max_{j=1, \dots, J} N_{z_j}$  and  $M_0 = \max_{j=1, \dots, J} M_{z_j}$ . Thus, for  $N > N_0$ ,  $\|\mathcal{R}_N(z_j)\| \leq M_0$  at these finitely many points.

For any  $z \in K$ , there exists  $z_j$  such that  $|z - z_j| < \varepsilon$ . Using the *first resolvent identity*:

$$\mathcal{R}_N(z) - \mathcal{R}_N(z_j) = \mathcal{R}_N(z)(z - z_j)\mathcal{R}_N(z_j),$$

we obtain:

$$\|\mathcal{R}_N(z) - \mathcal{R}_N(z_j)\| \leq \|\mathcal{R}_N(z)\| \|\mathcal{R}_N(z_j)\| |z - z_j| < \|\mathcal{R}_N(z)\| M_0 \varepsilon.$$

So, we have shown that  $\mathcal{R}(z)$  is continuous in  $z \in U$ , and thus  $\|\mathcal{R}(z)\|$  is bounded on  $U$ . Next,

$$\|\mathcal{R}_N(z)\| \leq \|\mathcal{R}_N(z) - \mathcal{R}_N(z_j)\| + \|\mathcal{R}_N(z_j)\| \leq \|\mathcal{R}_N(z)\| M_0 \varepsilon + M_0.$$

After rearranging, we have:

$$\|\mathcal{R}_N(z)\| (1 - M_0 \varepsilon) \leq M_0.$$

Choose  $\varepsilon > 0$  such that  $M_0 \varepsilon < 1$  (e.g.,  $\varepsilon < 1/(M_0 + 1)$ ), ensuring  $1 - M_0 \varepsilon > 0$ . Then

$$\|\mathcal{R}_N(z)\| \leq \frac{M_0}{1 - M_0 \varepsilon}.$$

Let  $M_U := \frac{M_0}{1 - M_0 \varepsilon}$ , which depends only on  $U$ , we finish the proof.  $\square$

**Lemma 4.7** ([3, Proposition 3.10]). Let  $\mathcal{P}$  and  $\mathcal{P}_N$  (for  $n \in \mathbb{N}$ ) be projections such that  $\mathcal{P}_N$  converges to  $\mathcal{P}$  pointwise, and let  $\dim \mathcal{P}\mathcal{F} < \infty$ . Then,  $\|(\mathcal{P} - \mathcal{P}_N)\mathcal{P}\| \rightarrow 0$  as  $N$  becomes sufficiently large, and for  $N$  large enough,  $\dim \mathcal{P}_N\mathcal{F} \geq \dim \mathcal{P}\mathcal{F}$ .

**Remark 4.8.** In many numerical methods, particularly those that rely on projecting infinite-dimensional problems onto finite-dimensional subspaces (e.g. Galerkin approximation), Lemma 4.7 plays a fundamental role in ensuring stability and consistency of approximations. It guarantees that once  $\mathcal{P}_N$  converges strongly to a limiting projector  $\mathcal{P}$ , the dimension of the projected subspace  $\mathcal{P}_N\mathcal{F}$  cannot suddenly drop below the dimension of  $\mathcal{P}\mathcal{F}$ . This means that the subspace capturing the “essential” part of the solution does not degenerate.

**Corollary 4.9.** Suppose Eq.(7) in Assumption 4.2 holds for all  $z \in \Gamma$ . Then,  $\dim \mathcal{P}_N\mathcal{F} \geq \dim \mathcal{P}\mathcal{F}$ , for  $N$  large enough.

*Proof.* For any  $f \in \mathcal{F}$ , we have

$$\mathcal{P}_N f - \mathcal{P} f = \frac{1}{2\pi i} \int_{\Gamma} [\mathcal{R}_N(z) - \mathcal{R}(z)] x dz.$$

Using the resolvent identity, whenever  $N$  is large enough we get

$$\begin{aligned} \|\mathcal{P}_N f - \mathcal{P} f\| &= \left\| \frac{1}{2\pi i} \int_{\Gamma} \mathcal{R}_N(z) (\mathcal{K} - \mathcal{K}_N) \mathcal{R}(z) f dz \right\| \\ &\leq \frac{|\Gamma|}{2\pi} \sup_{z \in \Gamma} \|\mathcal{R}_N(z)\| \cdot \sup_{z \in \Gamma} \|(\mathcal{K} - \mathcal{K}_N) \mathcal{R}(z) x\|, \end{aligned}$$

Thus, by Lemma 4.7, we have  $\dim \mathcal{P}_N\mathcal{F} \geq \dim \mathcal{P}\mathcal{F}$ , for  $N$  large enough.  $\square$

**Theorem 4.10.** Let  $\lambda$  be an isolated eigenvalue of  $\mathcal{K}$  with finite algebraic multiplicity  $m$ . Let  $\Gamma \subset \rho(\mathcal{K})$  be a closed Jordan curve enclosing  $\lambda$  such that  $\sigma(\mathcal{K}) \cap \Delta = \{\lambda\}$ , where  $\Delta$  is the region inside  $\Gamma$ . Suppose Assumption 4.2 holds for all  $z \in \Gamma$ . Then we have

$$\lim_{N \rightarrow \infty} [\sigma(\mathcal{K}_N) \cap \Delta] = \{\lambda\}$$

in the Kuratowski sense [3, Chapter 5.1.1] (hence, implying Hausdorff convergence). Moreover, if Assumption 4.5 holds, we have  $\sigma(\mathcal{K}_N) \cap \Delta$  consists of exactly  $m$  eigenvalues, for  $N$  large enough.

**Proof of Theorem 4.10.** We will first show the lower semicontinuity and upper semicontinuity (See Remark 4.11), which implies the Hausdorff convergence, then we will show that the algebraic multiplicity is preserved. Let  $\mathcal{P}$  and  $\mathcal{P}_N$  be the spectral projections of  $\mathcal{K}$  and  $\mathcal{K}_N$  associated with  $\lambda$  and  $\sigma(\mathcal{K}_N) \cap \Delta$ , respectively.

**Lower Semicontinuity:** Choose  $\varepsilon > 0$  small enough so that  $\Delta_{\varepsilon} = \Delta - \{z : |z - \lambda| < \varepsilon\}$  and the circle  $\gamma_{\varepsilon} = \{z : |z - \lambda| = \varepsilon\}$  are in  $\rho(\mathcal{K})$ . Stability from Lemma 4.6 ensures a bound  $\sup_{z \in \Delta_{\varepsilon}} \|\mathcal{R}_N(z)\| \leq M(\varepsilon)$  for  $N > N(\varepsilon)$ . By Corollary 4.9,  $\dim \mathcal{P}_N^{\gamma_{\varepsilon}} \mathcal{F} \geq m$  for  $N > N(\varepsilon)$  implies  $\sigma(\mathcal{K}_N) \cap \{z : |z - \lambda| < \varepsilon\} \neq \emptyset$ . Thus, there exists  $\lambda_N \in \sigma(\mathcal{K}_N) \cap \Delta$  with  $|\lambda_N - \lambda| < \varepsilon$  for large  $N$ , confirming  $\lambda$  as a limit point.

**Upper Semicontinuity:** Lemma 4.6 ensures  $\Delta_{\varepsilon} \subset \rho(\mathcal{K}_N)$  for  $N > N(\varepsilon)$ , so  $\sigma(\mathcal{K}_N) \cap \Delta_{\varepsilon} = \emptyset$ . Hence, any  $\mu \in \sigma(\mathcal{K}_N) \cap \Delta$  satisfies  $|\mu - \lambda| < \varepsilon$ . As  $\varepsilon \rightarrow 0$ , any subsequence of  $\mu$  converges to  $\lambda$ .

**Multiplicity Preservation:** Suppose Assumption 4.5 holds. Now we show that  $\sigma(\mathcal{K}_N) \cap \Delta$  consists of exactly  $m$  eigenvalues, counting algebraic multiplicities. By [3, Theorem 2.27],  $\sigma(\mathcal{K}_N) \cap \Delta$  is the spectrum of  $\mathcal{P}_N \mathcal{K}_N \mathcal{P}_N$  on

$\mathcal{P}_N \mathcal{F}$ . Since  $\dim \mathcal{P}_N \mathcal{F} = m < \infty$ ,  $\mathcal{P}_N \mathcal{K}_N \mathcal{P}_N$  is a finite-dimensional operator with at most  $m$  eigenvalues (counting multiplicities). If there were more,  $\dim \mathcal{P}_N \mathcal{F} > m$ , contradicting the assumption; if fewer,  $\dim \mathcal{P}_N \mathcal{F} < m$ , also a contradiction for large  $n$ . Thus,  $\sigma(\mathcal{K}_N) \cap \Delta$  consists of exactly  $m$  eigenvalues, which preserves the algebraic multiplicity.  $\square$

**Remark 4.11.** Intuitively speaking, upper semicontinuity ensures that every limit of approximate spectral points is contained in the true spectrum, which prevents irrelevant points (i.e., *spectral pollution*) and lower semicontinuity ensures that every point of the true spectrum is approached by some approximate spectral points, which prevents loss of spectral points (i.e., *spectral inclusion*).

**Remark 4.12.** The [3, Theorem 2.27] in the above theorem mainly says that one can construct a spectral projection via a contour integral, which decomposes the space into two invariant subspaces: one that contains exactly the isolated part of the spectrum and one that contains the remainder. Essentially, it provides a method to “split” or reduce  $\mathcal{K}$  into simpler parts corresponding to these separated spectral regions.

**Remark 4.13.** In a compact metric space (or for compact sets), Kuratowski convergence implies Hausdorff convergence because the topological constraints (via lower and upper limits) force the sets to become metrically close in the Hausdorff distance.

Now we want to extend the Hausdorff convergence result beyond isolated eigenvalues to a compact subset of the spectrum. In order to do so, we need to introduce a new concept called *resolvent stability* as following.

**Definition 4.14** (Resolvent Stability). Let  $\{\mathcal{K}_N\}$  be a sequence of closed linear operators on a Banach space  $\mathcal{F}$ , and let  $U$  be a compact subset of  $\mathbb{C}$ . The sequence  $\{\mathcal{K}_N\}$  is said to be *resolvent stable around  $U$*  if there exists a neighborhood  $N(U)$  of  $U$  such that for any  $z \in N(U) \setminus U$ , we have

$$\liminf_{N \rightarrow \infty} \text{dist}(\sigma(\mathcal{K}_N), z) > 0 \Rightarrow \limsup_{N \rightarrow \infty} \|\mathcal{R}(z, \mathcal{K}_N)\| < \infty.$$

**Remark 4.15.** Equivalently speaking, we can also say that  $N(U) \setminus U$  has the  $\{\mathcal{K}_N\}$ -*Resolvent Condition*, where the  $\{\mathcal{K}_N\}$ -*Resolvent Condition* for a point  $z \in \mathbb{C}$  means that

$$\liminf_{N \rightarrow \infty} \text{dist}(\sigma(\mathcal{K}_N), z) > 0 \Rightarrow \limsup_{N \rightarrow \infty} \|\mathcal{R}(z, \mathcal{K}_N)\| < \infty.$$

The *resolvent stability* property prevents the formation of spurious eigenvalues in the vicinity of the compact subset  $U$ , which is necessary for proving the lower semicontinuity in the spectral convergence.

**Theorem 4.16.** Let  $\mathcal{K}$  be a bounded Koopman operator and  $\{\mathcal{K}_N\}_{N \in \mathbb{N}}$  be finite-dimensional approximations that satisfy Assumption 4.2. Let  $U \subset \sigma(\mathcal{K})$  be a non-empty compact subset enclosed by a positively oriented contour  $\Gamma \subset \rho(\mathcal{K})$ , and let  $\Delta$  denote the interior of  $\Gamma$ . Then

$$\liminf_{N \rightarrow \infty} \text{dist}(U, \sigma(\mathcal{K}_N) \cap \Delta) = 0,$$

i.e. the spectrum of  $\mathcal{K}_N$  is lower semicontinuous at  $U$ .

*Proof.* Because  $\Delta \setminus U \subset \rho(\mathcal{K})$ , every  $z \in \Delta \setminus U$  lies in the resolvent set of  $\mathcal{K}$ . Assumption 4.2 therefore yields constants  $N_z \in \mathbb{N}$  and  $M_z > 0$  such that for all  $N > N_z$ ,

$$z \in \rho(\mathcal{K}_N) \quad \text{and} \quad \|\mathcal{R}_N(z)\| \leq M_z,$$

where  $\mathcal{R}_N(z) = (zI - \mathcal{K}_N)^{-1}$ . Fix  $z \in \Delta \setminus U$  and assume  $\liminf_{N \rightarrow \infty} \text{dist}(\sigma(\mathcal{K}_N), z) > 0$ . Then there exist  $\delta > 0$  and  $N_0$  such that  $\text{dist}(\sigma(\mathcal{K}_N), z) > \delta$  for all  $N > N_0$ . Consequently, for every  $N > \max\{N_0, N_z\}$  we have the uniform bound  $\|\mathcal{R}_N(z)\| \leq M_z$ . Hence the sequence  $\{\mathcal{K}_N\}$  is *resolvent-stable* around  $U$  in the sense of Definition 4.14. Applying Mills [20, Theorem 3.2] gives  $\liminf_{N \rightarrow \infty} \text{dist}(U, \sigma(\mathcal{K}_N) \cap \Delta) \rightarrow 0$ , which is exactly the desired lower semicontinuity.  $\square$

**Remark 4.17.** Upper semicontinuity in Theorem 4.16 is not satisfied unless we have a stronger condition that  $\mathcal{K}_N$  uniformly converges to  $\mathcal{K}$ . Refer to [11, Theorem 3.1, Chapter 4] for more details.

We want to point out that Chatelin’s work in [3] primarily addresses the convergence of isolated eigenvalues which provides a comprehensive framework that ensures preservation of algebraic multiplicities during the approximation process. This is particularly valuable for numerical analysis as it guarantees that the number of approximate eigenvalues (counting multiplicity) matches that of the exact operator. In contrast, Mills’ work in [20] extends spectral convergence theory (i.e., lower semicontinuity) to compact subsets of the spectrum, which offers a much broader applicability beyond just isolated eigenvalues.

## 5 Error Bounds Analysis

In last section, we established the convergence of the approximated spectrum  $\sigma(\mathcal{K}_N)$  to the true spectrum  $\sigma(\mathcal{K})$ . However, for practical application, it is essential to quantify the error of a computed solution. In this section, we will derive an error bound for the computed eigenvalues that is controlled by a computable residual quantity  $\eta_N$ , as defined later. This provides a practical way to assess the accuracy of the spectral information obtained via Galerkin methods such as EDMD [28] and our pseudo-resolvent approach.

**Definition 5.1** (Arithmetic Mean of Approximate Eigenvalues). Let  $\lambda$  be an isolated eigenvalue of  $\mathcal{K}$  with algebraic multiplicity  $m_\lambda$ , and let  $\Gamma_\lambda$  be an isolating closed Jordan curve as defined in Definition 4.4. For  $N$  large enough, Assumption 4.5 guarantees that there are exactly  $m_\lambda$  eigenvalues of  $\mathcal{K}_N$  inside  $\Gamma_\lambda$ , which we denote by  $\{\mu_{N,j}\}$  for  $j = 1, \dots, m_\lambda$ , counting multiplicities. We define their arithmetic mean as:

$$\bar{\lambda}_N := \frac{1}{m_\lambda} \sum_{j=1}^{m_\lambda} \mu_{N,j}. \quad (9)$$

**Definition 5.2.** Let  $\mathcal{P}_N^\lambda$  be the spectral projection associated with the eigenvalues of  $\mathcal{K}_N$  inside the contour  $\Gamma_\lambda$ . We define the computable residual quantity  $\eta_N$  as:

$$\eta_N := \|(\mathcal{K} - \mathcal{K}_N)\mathcal{P}_N^\lambda\|. \quad (10)$$

To support our main proof, we state a key lemma from spectral approximation theory in the following which establishes the fundamental relationship between the error in the mean eigenvalue and the trace of an operator difference.

**Lemma 5.3** ([3, Lemma 6.2]). Let  $\lambda$  be an isolated eigenvalue of  $\mathcal{K}$  with finite algebraic multiplicity  $m$ , and  $\mathcal{M}$  be the associated invariant subspace. Consider the operator  $\mathcal{G}_N := \mathcal{K}_N|_{\mathcal{M}}$ , which is the restriction of the Galerkin approximation  $\mathcal{K}_N$  to the true invariant subspace  $\mathcal{M}$ . Let  $\bar{\lambda}$  be the arithmetic mean of the  $m$  eigenvalues of the finite-dimensional operator  $\mathcal{G}_N$ . Denoting these eigenvalues by  $\{\mu_{N,j}\}_{j=1}^m$ , the arithmetic mean is defined as:

$$\bar{\lambda} := \frac{1}{m} \sum_{j=1}^m \mu_{N,j}.$$

Then, we have the following identity:

$$\lambda - \bar{\lambda} = \frac{1}{m} \text{tr}((\mathcal{K} - \mathcal{K}_N)|_{\mathcal{M}}).$$

**Theorem 5.4.** Let  $\lambda$  be an isolated eigenvalue of the Koopman operator  $\mathcal{K}$  with finite algebraic multiplicity  $m_\lambda$ . Let  $\Gamma_\lambda$  be a closed Jordan curve isolating  $\lambda$  from the rest of  $\sigma(\mathcal{K})$ . Suppose that Assumption 4.2 and Assumption 4.5 hold, then for  $N$  sufficiently large, the error in the arithmetic mean of the approximate eigenvalues is bounded by the computable residual  $\eta_N$ , as given in the Definition 5.2. Specifically, there exists a constant  $C$  independent of  $N$  such that:

$$|\lambda - \bar{\lambda}_N| \leq C \cdot \eta_N.$$

*Proof.* Let  $\mathcal{M}_N^\lambda := \mathcal{P}_N^\lambda \mathcal{F}$  be the  $m_\lambda$ -dimensional approximate invariant subspace. Define the operators  $\mathcal{G}_N := \mathcal{K}_N|_{\mathcal{M}_N^\lambda}$  and  $\mathcal{H}_N := \mathcal{P}_N^\lambda \mathcal{K} \mathcal{P}_N^\lambda$ . The arithmetic mean  $\bar{\lambda}_N$  satisfies  $\bar{\lambda}_N = \frac{1}{m_\lambda} \text{tr}(\mathcal{G}_N)$  and the error bound derives from the trace difference satisfies  $|\text{tr}(\mathcal{H}_N - \mathcal{G}_N)| \leq m_\lambda \cdot \|\mathcal{P}_N^\lambda(\mathcal{K} - \mathcal{K}_N)\mathcal{P}_N^\lambda\|$  by Lemma 5.3. Then, by uniform boundedness of  $\|\mathcal{P}_N^\lambda\| \leq C$  (from Assumption 4.5) and [3, Theorem 6.15], we obtain the following result:

$$|\lambda - \bar{\lambda}_N| \leq C \cdot \|(\mathcal{K} - \mathcal{K}_N)\mathcal{P}_N^\lambda\| = C \cdot \eta_N.$$

□

## 6 Experiments

### 6.1 Pendulum

In this experiment, data is generated by simulating a single pendulum system. In the simulation setting, a single trajectory of 1500 time steps is produced with a fixed sampling time step of 0.2 seconds. The simulation starts from a randomly initialized state where the angle  $\theta$  is chosen uniformly from 0 to  $2\pi$  and its angular velocity  $\dot{\theta}$  from -5 to 5. The system's dynamics are governed by the equation

$$\ddot{\theta} = -\frac{3g}{2l} \sin(\theta)$$

with the parameters set as follows: gravitational acceleration  $g = 9.8$  and pendulum length  $l = 1.0$ . At each time step, the angular acceleration is calculated using this equation, and then the angular velocity and angle are updated via Euler's method. To select the dictionary, we use two sets of basis functions: a Fourier basis for the angle  $\theta$  and a Hermite polynomial basis for the angular velocity  $\dot{\theta}$ . Specifically, the Fourier basis is constructed using complex exponentials  $\exp\{in\theta\}$  for  $n$  ranging from  $-20$  to  $20$ , and the Hermite basis employs Hermite polynomials evaluated up to order  $30$  (with the velocity  $\dot{\theta}$  rescaled by  $1/\sqrt{2}$ ). These basis functions are multiplied to form a dictionary of observables, which is then used to approximate the resolvent of the Koopman operator and study the system's spectral properties.

In Figure 1, we illustrate the behavior of  $1/\|\mathbf{R}(z, \mathbf{K}_N)\|$  as the grid point  $z$  varies across these circles with radii  $\Gamma_{1.01}$ ,  $\Gamma_{1.1}$ , and  $\Gamma_{1.5}$ . Theoretically, the inverse of the spectral norm of the resolvent should approach zero as  $z$  gets closer to the unit circle, where the true spectrum of the Koopman operator for this pendulum system is expected to locate. This is observed in the figure that the value of  $1/\|\mathbf{R}(z, \mathbf{K}_N)\|$  decreases as the radius approaches 1. Consequently, by setting a smaller threshold for detection, only grid points nearer to the unit circle are identified as part of the spectrum, which enhances the accuracy of the spectral approximation.

In Figure 2, we approximate the Koopman operator  $\mathbf{K}_N$  via EDMD and the resolvent operator  $\mathbf{R}(z, \mathbf{K}_N)$  using our method with dictionary sizes of 441, 600, and 806 basis functions, respectively, on another simulated dataset. The grid points  $z$  are chosen along the circle  $\Gamma_{1.01}$ , a slight perturbation of the unit circle to avoid singularity when computing  $\|\mathbf{R}(z, \mathbf{K}_N)\|$ . As the dictionary size  $N$  increases,  $1/\|\mathbf{R}(z, \mathbf{K}_N)\|$  becomes smaller for a larger number of grid point  $z$ , thus leading to more points being detected as part of the approximated spectrum along the circle  $\Gamma_{1.01}$  for a fixed threshold. This trend suggests a convergence behavior as  $N$  grows.

In Figure 3, We also have tested for the generator as computed in Eq.(6). In continuous time case, since the spectrum of the Koopman operator is the unit circle, the corresponding spectrum for the Koopman generator  $\mathcal{A}$  should be the imaginary axis. In the first figure, the spectrum is computed by gEDMD [14]. Since our basis functions, i.e., the Fourier basis, are selected from the frequency close to 0, this explains that the evaluation for  $z$  closer to 0 is more accurate, in other words,  $1/\|\mathbf{R}(z, \mathbf{A}_N)\|$  is smaller for  $z$  closer to 0.

## 6.2 Comparing pseudospectra contour

In this subsection, we compare the spectral approximation capabilities of ResDMD and the proposed Resolvent DMD by examining their pseudospectral contours. The primary objective is to demonstrate the robustness of each method against spectral pollution and their ability to localize spectral components in the complex plane, particularly in regions away from the origin.

We consider the Lorenz 63 system, governed by the following differential equations:

$$\begin{aligned}\dot{x} &= \sigma(y - x), \\ \dot{y} &= x(\rho - sz) - y, \\ \dot{z} &= sxy - \beta z,\end{aligned}\tag{11}$$

where the system parameters are set to  $\sigma = 10.0$ ,  $\beta = 8/3$ , and  $\rho = 40.0$ , corresponding to a chaotic regime. A scaling factor  $s = 0.1$  is introduced to the nonlinear coupling terms to adjust the dynamic range of the state variables. Time-series data are generated by integrating a single trajectory with a time step of  $\Delta t = 0.05$ .

For the construction of the Koopman operator approximation, we employ a dictionary consisting of tensor products of normalized Hermite polynomials. To efficiently manage the dimensionality while capturing the essential dynamics, the basis functions are selected via a hyperbolic-cross truncation of the multi-index set. This procedure results in a dictionary size of  $N = 110$ . Inner products are approximated using Gauss–Hermite quadrature.

We analyze the pseudospectra contours for both methods, which are computed as the level sets of the inverse of the resolvent norm,  $1/\|\mathbf{R}_N(z)\|$ . This quantity serves as a reliable indicator of the approximate spectrum; regions with large resolvent norms (i.e., small inverse values) correspond to the location of spectral points.

Figure 4 presents the comparison of pseudospectral contours computed using ResDMD (left) and Resolvent DMD (right). In the ResDMD result, the contours exhibit irregular distortions and isolated "islands" in the complex plane, indicating the presence of spurious eigenvalues and spectral pollution. In contrast, the Resolvent DMD result displays smooth contours that are sharply localized along the real axis. This indicates that Resolvent DMD more accurately recovers the spectral components of the continuous-time generator, which typically lie along the real axis for dissipative chaotic attractors, and effectively suppresses the spectral pollution observed in ResDMD.

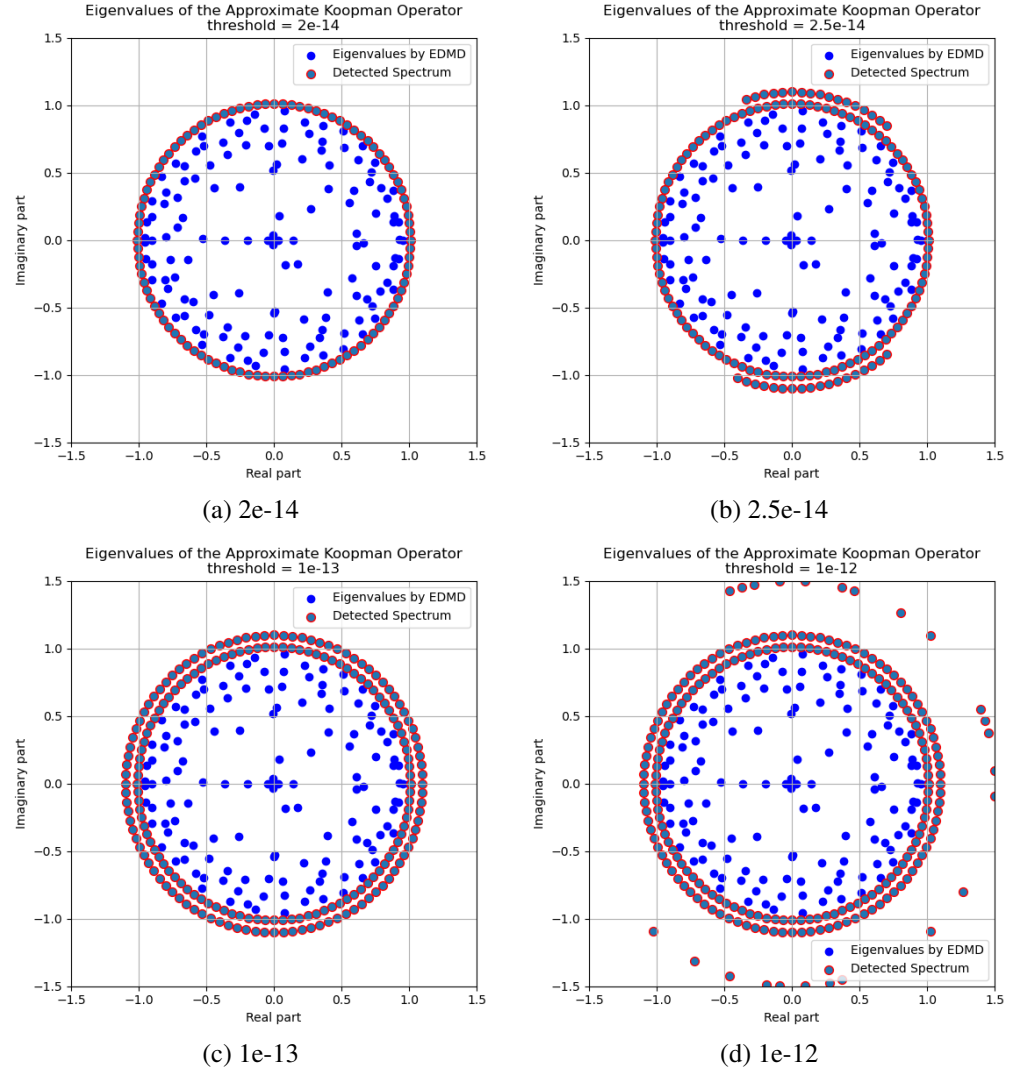


Figure 1: As  $z$  approaches the unit circle, the value of  $1/\|\mathbf{R}(z, \mathbf{K}_N)\|$  decreases.

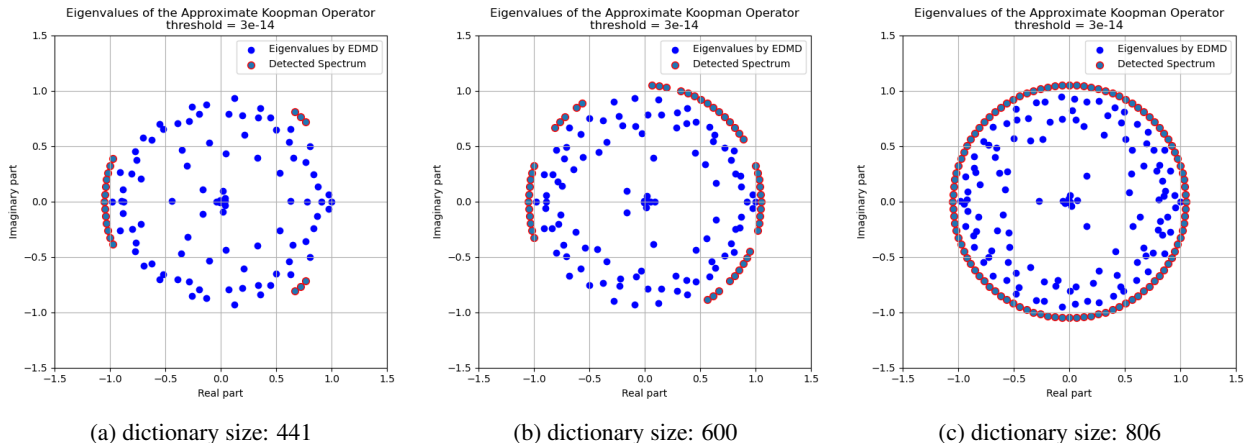


Figure 2: Effect of increasing the dictionary size  $N$  (number of basis functions) on the detection of spectral points.

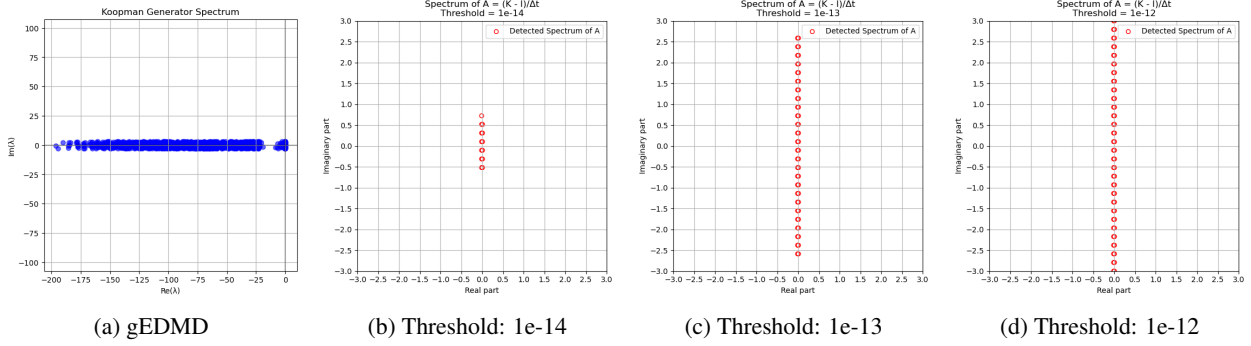


Figure 3: Evaluation of  $1/\|\mathbf{R}(x, \mathbf{A}_N)\|$  at  $x = \pm 0.01$ .

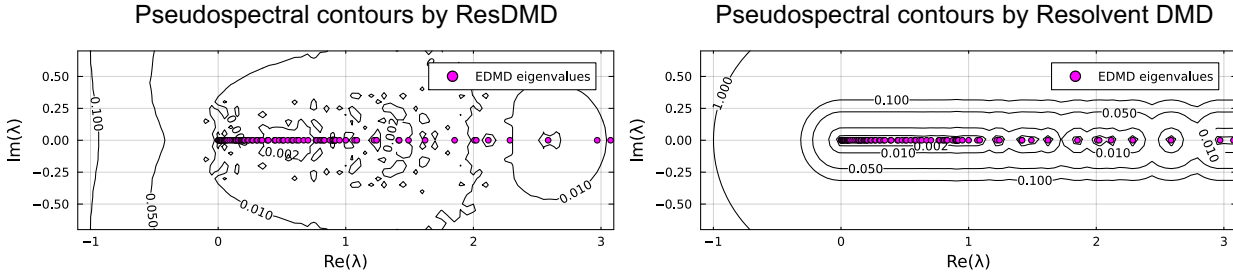


Figure 4: Pseudospectral contours computed by ResDMD (left) and Resolvent DMD (right) for the Lorenz system. The contours represent the level sets of the inverse resolvent norm,  $1/\|\mathbf{R}_N(z)\|$ . The pink dots indicate the eigenvalues computed by standard EDMD. Resolvent DMD demonstrates sharper localization along the real axis with significantly reduced spectral pollution compared to the distortions observed in ResDMD.

### 6.3 Clustering two oscillators with thermal noise

We next compare Resolvent DMD with ResDMD on a pair of weakly damped oscillators observed under thermal and measurement noise. Both methods are designed to suppress spectral pollution, but this example probes their ability to separate two physical modes whose spectral supports are close and therefore difficult to distinguish.

We consider two second-order oscillators with viscous damping and additive thermal noise,

$$\ddot{x}_1(t) = -2\zeta\omega_1\dot{x}_1(t) - \omega_1^2x_1(t) + \sigma_1\eta_1(t), \quad (12)$$

$$\ddot{x}_2(t) = -2\zeta\omega_2\dot{x}_2(t) - \omega_2^2x_2(t) + \sigma_2\eta_2(t), \quad (13)$$

with  $\omega_1 = 3\pi/5$ ,  $\omega_2 = 3 \cdot 2\pi/5$ , damping ratio  $\zeta = 0.2$ , and noise intensities  $\sigma_1 = 0.05$ ,  $\sigma_2 = 0.15$ . The observed scalar signal is

$$x(t) = x_1(t) + x_2(t) + \xi(t), \quad (14)$$

where  $\xi(t)$  is zero-mean Gaussian measurement noise with standard deviation 0.015. We integrate the stochastic system on  $[0, 190]$  with time step  $\Delta t = 0.1$  and subsample to obtain  $M = 1050$  snapshots. From this single noisy trajectory we construct time-delay embedded data matrices  $\Psi_X, \Psi_Y$  of width  $N = 850$ .

Using quadrature-weighted inner products, we form the Gram matrix  $G = \Psi_X^* W \Psi_X$  and the cross matrix  $A = \Psi_X^* W \Psi_Y$ , where  $W = \text{diag}(w_m)$  contains the snapshot weights. The entries  $G_{i,j} = \langle \psi_i, \psi_j \rangle$  and  $A_{i,j} = \langle \mathcal{K}\psi_i, \psi_j \rangle$  define a finite-dimensional Galerkin approximation of the Koopman operator, and we obtain a matrix approximation

$$\mathcal{K}_N = G^\dagger A \approx (\Psi_X^* W \Psi_X)^\dagger (\Psi_X^* W \Psi_Y). \quad (15)$$

Throughout this example we take  $w_m = 1/M$  for randomly sampled snapshots [13, 17].

In our setting, both ResDMD and the proposed Resolvent DMD are designed to evaluate, from data, the spectrum of the Koopman operator—including its continuous component—but they do so using different constructions. ResDMD constructs, for each point  $z$  in the complex plane, a residual which, up to known scaling factors, is essentially the reciprocal of the resolvent norm of the Koopman operator. Resolvent DMD instead works directly with the finite-dimensional resolvent approximation  $\mathbf{R}_N(z)$  defined in Eq. (4) and Eq. (5). For each  $z$ , we take the dominant

eigendirection of this resolvent (the eigenvector associated with its largest amplification) and regard the corresponding dictionary-based observable as a pseudoeigenfunction. Thus, the two methods approximate the same underlying resolvent quantity via reciprocal summaries: ResDMD uses residuals, whereas Resolvent DMD acts directly on the resolvent and its dominant eigendirections. In the present two-oscillator experiment, this direct resolvent-based construction yields a more accurate finite-dimensional approximation and, as we show below, a clearer separation of nearby spectral components than the residual-based ResDMD surrogate.

To compare the dynamic features extracted by ResDMD and Resolvent DMD, we follow the clustering framework in [23]. For each method, we collect a family of pseudoeigenfunctions  $g_{(z)}$  over a grid of  $z$  in the complex plane. We then compute kernel principal angles between the subspaces spanned by these pseudoeigenfunctions, construct a similarity matrix from these angles, and apply spectral clustering to obtain a low-dimensional feature representation. Finally, we perform fuzzy C-means clustering in this embedded feature space to account for ambiguity induced by continuous spectra and obtain three clusters that we interpret as candidate dynamic components.

Figure 5 shows the clustering results in the embedded feature space for ResDMD (left) and Resolvent DMD (right). In the Resolvent DMD case, the three clusters occupy well-separated regions, with clear gaps between the groups associated with the two physical modes and the residual high-frequency/noise-like components. In contrast, for ResDMD the regions corresponding to Cluster 2 and Cluster 3 lie in a largely overlapping portion of the feature space, and their boundary is much less distinct. This indicates that, although both methods are based on the same resolvent of the Koopman operator, the pseudoeigenfunctions produced by Resolvent DMD are more cleanly partitioned into three coherent groups in the embedded space, while the ResDMD pseudoeigenfunctions exhibit stronger mixing between two of the clusters.

To compare the dynamic features extracted by ResDMD and Resolvent DMD, we follow the clustering framework in [23]. For each method, we collect a family of pseudoeigenfunctions  $g_{(z)}$  over a grid of  $z$  in the complex plane. We then compute kernel principal angles between the subspaces spanned by these pseudoeigenfunctions, construct a similarity matrix from these angles, and apply spectral clustering to obtain a low-dimensional feature representation. Finally, we perform fuzzy C-means clustering in this embedded feature space to account for ambiguity induced by continuous spectra and obtain three clusters that we interpret as candidate dynamic components.

Figure 5 shows the clustering results in the embedded feature space for ResDMD (left) and Resolvent DMD (right). In the Resolvent DMD case, the three clusters occupy well-separated regions, with clear gaps between the groups associated with the two physical modes and the residual high-frequency/noise-like components. In contrast, for ResDMD the regions corresponding to Cluster 2 and Cluster 3 lie in a largely overlapping portion of the feature space, and their boundary is much less distinct. This indicates that, although both methods are based on the same resolvent of the Koopman operator, the pseudoeigenfunctions produced by Resolvent DMD are more cleanly partitioned into three coherent groups in the embedded space, while the ResDMD pseudoeigenfunctions exhibit stronger mixing between two of the clusters.

To connect the clustering in the embedded space with spectral information, we compute spectral measures from the pseudoeigenfunctions using the rigorous resolvent-based procedure developed in [4]. Figure 6 shows the resulting spectral measures colored by cluster labels for ResDMD (left) and Resolvent DMD (right). In the Resolvent DMD case, the two broad peaks associated with the physical oscillation frequencies are each assigned predominantly to a distinct cluster, and a third cluster captures the remaining higher-frequency components. Thus the cluster structure aligns well with the two physical spectral peaks. In the ResDMD case, however, the cluster assignment on the low-frequency side is substantially mixed: the spectral contribution around the lower physical peak is not cleanly separated from nearby components, and the resulting clusters no longer correspond clearly to the two physical modes. This suggests that, when two physical modes occupy nearby spectral regions, Resolvent DMD has higher discriminative power than ResDMD in separating those modes, even though both methods share the goal of mitigating spectral pollution.

Finally, Figure 7 examines the cluster assignments at the level of the original time series. For each method, we reconstruct mode contributions by projecting the signal onto the clustered pseudoeigenfunctions and summing the components within each cluster. In the ResDMD reconstruction (left), the mode associated with the low-frequency cluster does not reproduce the correct low-frequency behavior; leakage from other components is visible, consistent with the failure to isolate the lower spectral peak in Figure 6. By contrast, the Resolvent DMD reconstruction (right) yields two components that closely match the two physical modes in both frequency and temporal modulation. These reconstructions corroborate the spectral-measure analysis and indicate that, in this example with two nearby spectral bands, Resolvent DMD achieves a more reliable separation of physical modes than ResDMD, while still pursuing the shared objective of suppressing spectral pollution.

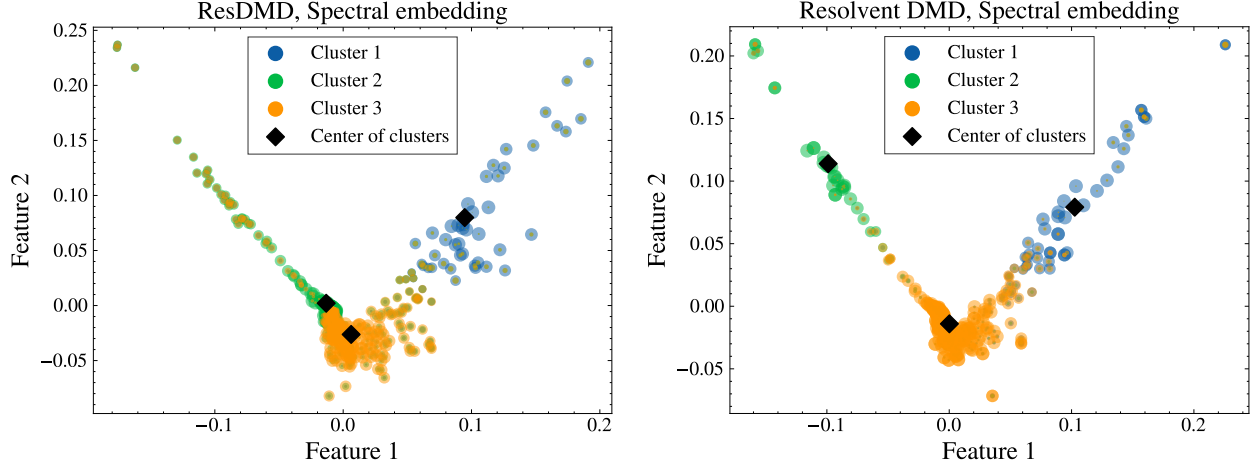


Figure 5: Clustering in the embedded feature space for ResDMD (left) and Resolvent DMD (right). Resolvent DMD produces three clearly separated clusters, whereas for ResDMD the regions corresponding to Cluster 2 and Cluster 3 lie close together with a blurred boundary.

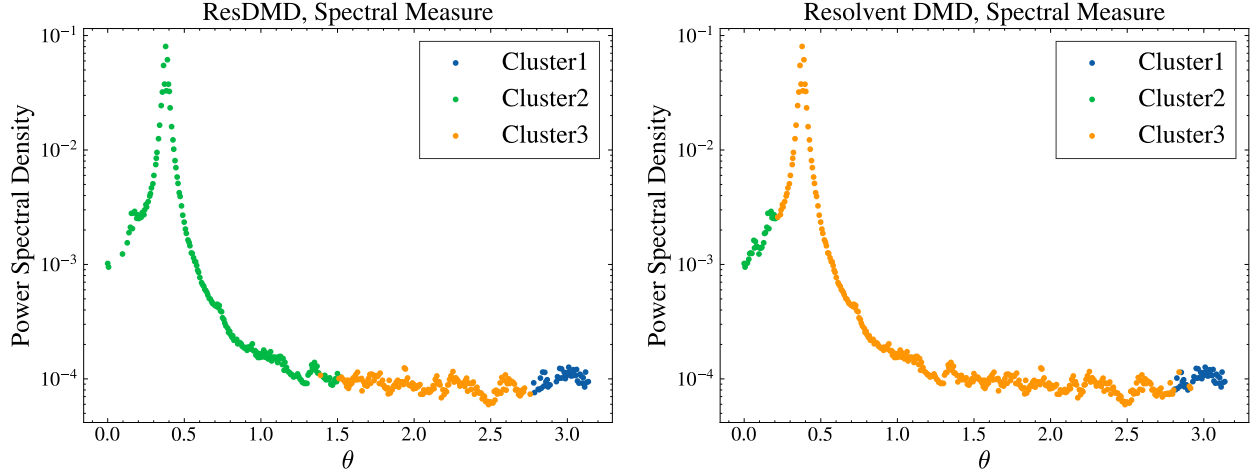


Figure 6: Clustering of spectral measures for ResDMD (left) and Resolvent DMD (right), computed using the resolvent-based procedure of [4]. Resolvent DMD separates the two physical peaks into distinct clusters, whereas ResDMD does not clearly isolate the lower-frequency peak.

## 7 Conclusion

In this work, we have presented a novel data-driven framework for the spectral analysis of the Koopman operator through the lens of pseudo-resolvents. By leveraging the Sherman-Morrison-Woodbury identity, we constructed a direct matrix approximation of the resolvent operator based on Galerkin approximations for spectral detection. Our theoretical analysis establishes that the proposed method ensures spectral convergence in the Hausdorff metric under the resolvent stability conditions. Furthermore, we derived rigorous error bounds for the arithmetic mean of approximate eigenvalues, controlled by a computable residual quantity  $\eta_N$ . This offers a quantifiable measure of reliability that is often missing in most other heuristic DMD approaches.

Several directions remain open for future work, including local error bounds for eigenfunction approximations, extension of the theoretical framework to continuous-time generators using semigroup theory, and the development of principled guidelines for dictionary selection that ensure the stable convergence assumption is satisfied.

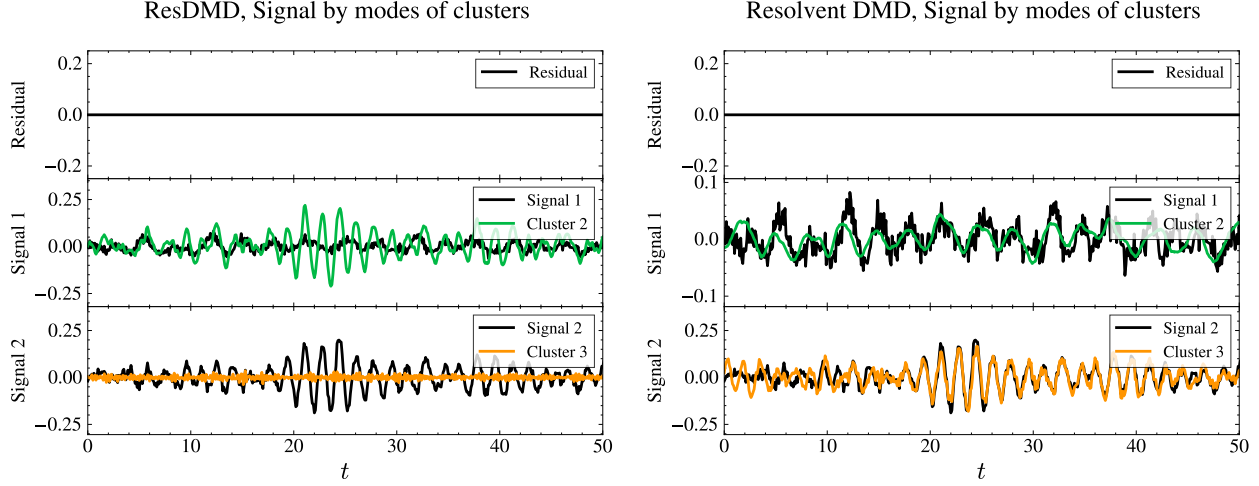


Figure 7: Reconstruction of the original signal from clustered pseudoeigenfunctions for ResDMD (left) and Resolvent DMD (right). Resolvent DMD recovers the two physical modes accurately, whereas the ResDMD-based reconstruction fails to reproduce the low-frequency component.

## Acknowledgment

Y.X. and I.I. acknowledge support from JST CREST Grant Number JPMJCR24Q1 including AIP challenge program, Japan.

## References

- [1] DV Ansov. Geodesic flows on closed riemannian manifolds with negative curvature. In *Proc. Steklov Inst. Math.*, volume 90, pages 1–235, 1969.
- [2] George David Birkhoff. *Dynamical systems*, volume 9. American Mathematical Soc., 1927.
- [3] F. Chaitin-Chatelin. *Spectral Approximation of Linear Operators*. Computer science and applied mathematics. Academic Press, 1983.
- [4] Matthew J Colbrook and Alex Townsend. Rigorous data-driven computation of spectral properties of koopman operators for dynamical systems. *Communications on Pure and Applied Mathematics*, 77(1):221–283, 2024.
- [5] K.J. Engel, S. Brendle, R. Nagel, M. Campiti, T. Hahn, G. Metafune, G. Nickel, D. Pallara, C. Perazzoli, A. Rhandi, et al. *One-Parameter Semigroups for Linear Evolution Equations*. Graduate Texts in Mathematics. Springer New York, 1999.
- [6] Dimitrios Giannakis and Claire Valva. Consistent spectral approximation of koopman operators using resolvent compactification. *Nonlinearity*, 37(7):075021, 2024.
- [7] Philip Hartman. A lemma in the theory of structural stability of differential equations. *Proceedings of the American Mathematical Society*, 11(4):610–620, 1960.
- [8] Philip Hartman. *Ordinary differential equations*. SIAM, 2002.
- [9] Benjamin Herrmann, Peter J Baddoo, Richard Semaan, Steven L Brunton, and Beverley J McKeon. Data-driven resolvent analysis. *Journal of Fluid Mechanics*, 918:A10, 2021.
- [10] Isao Ishikawa, Yuka Hashimoto, Masahiro Ikeda, and Yoshinobu Kawahara. Koopman operators with intrinsic observables in rigged reproducing kernel hilbert spaces. *Nonlinearity*, 38(11):115022, 2025.
- [11] T. Kato. *Perturbation Theory for Linear Operators*. Classics in Mathematics. Springer Berlin Heidelberg, 1995.
- [12] Anatole Katok, AB Katok, and Boris Hasselblatt. *Introduction to the modern theory of dynamical systems*. Number 54. Cambridge university press, 1995.
- [13] Stefan Klus, Péter Koltai, and Christof Schütte. On the numerical approximation of the perron-frobenius and koopman operator. *arXiv preprint arXiv:1512.05997*, 2015.
- [14] Stefan Klus, Feliks Nüske, Sebastian Peitz, Jan-Hendrik Niemann, Cecilia Clementi, and Christof Schütte. Data-driven approximation of the koopman generator: Model reduction, system identification, and control. *Physica D: Nonlinear Phenomena*, 406:132416, 2020.
- [15] Bernard O Koopman. Hamiltonian systems and transformation in Hilbert space. *Proceedings of the National Academy of Sciences*, 17(5):315, 1931.
- [16] Bernard O. Koopman and John von Neumann. Dynamical systems of continuous spectra. *Proceedings of the National Academy of Sciences*, 18(3):255–263, 1932.
- [17] Milan Korda and Igor Mezić. On convergence of extended dynamic mode decomposition to the koopman operator. *Journal of Nonlinear Science*, 28:687–710, 2018.
- [18] Bethany Lusch, J Nathan Kutz, and Steven L Brunton. Deep learning for universal linear embeddings of nonlinear dynamics. *Nature communications*, 9(1):4950, 2018.
- [19] Igor Mezić. Spectral properties of dynamical systems, model reduction and decompositions. *Nonlinear Dynamics*, 41:309–325, 2005.
- [20] Wendell H. Mills, Jr. The resolvent stability condition for spectra convergence with application to the finite element approximation of noncompact operators. *SIAM J. Numer. Anal.*, 16(4):695–703, August 1979.
- [21] A. Pazy. *Semigroups of Linear Operators and Applications to Partial Differential Equations*. Applied Mathematical Sciences. Springer New York, 2012.
- [22] Henri Poincaré. Sur le problème des trois corps et les équations de la dynamique. *Acta mathematica*, 13(1):A3–A270, 1890.
- [23] Itsushi Sakata and Yoshinobu Kawahara. Enhancing spectral analysis in nonlinear dynamics with pseudoeigenfunctions from continuous spectra. *Scientific Reports*, 14(1):19276, 2024.
- [24] Stephen Smale. Differentiable dynamical systems. *Bulletin of the American mathematical Society*, 73(6):747–817, 1967.
- [25] Steven H Strogatz. *Nonlinear dynamics and chaos: with applications to physics, biology, chemistry, and engineering*. Chapman and Hall/CRC, 2024.

- [26] Yoshihiko Susuki, Alexandre Mauroy, and Igor Mezic. Koopman resolvent: A laplace-domain analysis of nonlinear autonomous dynamical systems. *SIAM Journal on Applied Dynamical Systems*, 20(4):2013–2036, 2021.
- [27] Jonathan H Tu. *Dynamic mode decomposition: Theory and applications*. PhD thesis, Princeton University, 2013.
- [28] Matthew O. Williams, Ioannis G. Kevrekidis, and Clarence W. Rowley. A data–driven approximation of the koopman operator: Extending dynamic mode decomposition. *Journal of Nonlinear Science*, 25(6):1307–1346, June 2015.
- [29] M.A. Woodbury and Princeton University. Department of Statistics. *Inverting Modified Matrices*. Memorandum Report / Statistical Research Group, Princeton. Department of Statistics, Princeton University, 1950.
- [30] Yuanchao Xu, Isao Ishikawa, Yuka Hashimoto, and Zhongwei Shen. A data-driven framework for koopman semigroup estimation in stochastic dynamical systems, 2025.